Journal of The Electrochemical Society

Performance and Durability of Proton Exchange Membrane Vapor-Fed Unitized Regenerative Fuel Cells

Journal of The Electrochemical Society, 2022 **169** 054514

Performance and Durability of Proton Exchange Membrane Vapor-Fed Unitized Regenerative Fuel Cells

Julie C. Fornaciari,[1,2,=,z] Samay Garg,[1,2,=,a] Xiong Peng,[1] Yagya N. Regmi,[3] Adam Z. Weber,[1] and Nemanja Danilovic[1]

[1]*Energy Storage and Distributed Resources Division, Lawrence Berkeley National Laboratory, Berkeley, California 94720, United States of America*
[2]*Department of Chemical and Biomolecular Engineering, University of California Berkeley, Berkeley, CA 94720, United States of America*
[3]*Manchester Fuel Cell Innovation Centre, Manchester Metropolitan University, Manchester M1 5GD, England, United Kingdom*

With a growing demand for electricity, clean hydrogen production and usage can be an asset not only to mitigate emissions but for long-term energy storage as well. Hydrogen gas, a high-density energy carrier, can be made through electrolysis in charging mode and generate electricity via a fuel cell in discharging mode in a unitized regenerative fuel cell (URFC). While URFCs reduce cost by combining the charging and discharging modes into a singular device, switching between modes becomes burdensome, and water management is a major challenge. One way to mitigate these issues is to operate the entire system in the vapor phase. Vapor-phase operation simplifies the physics of the system but will introduce losses within the system, primarily ohmic and mass transport during the charging mode. In this study, we explore the performance of a Proton-Exchange-Membrane (PEM)-URFC under vapor-phase conditions and the impact of different PEMs, feed gases, and relative humidity on the performance and durability. By tailoring operating conditions and membrane, the vapor-URFC achieves a roundtrip efficiency of 42% and a lifetime of 50,000 accelerated stress test cycles for fully humidified feeds. Discussion of vapor-URFC for energy storage and extensions to look at various applications shows the promise of this technology.
 [DOI: 10.1149/1945-7111/ac6c51]

Manuscript submitted February 18, 2022; revised manuscript received April 13, 2022. Published May 12, 2022. *This paper is part of the JES Focus Issue on Advanced Electrolysis for Renewable Energy Storage.*

Supplementary material for this article is available online

The prevalence of distributed renewable energy sources, primarily wind and solar, is growing rapidly, and so is the need for energy storage of these inherently intermittent resources. These energy-storage systems are a necessity to provide reliable, on-demand electricity, even seasonally, where solar energy can be stored from the summer to winter months.[1,2] Typical batteries, such as lithium-ion, are well-suited for short-term energy storage on the scale of hours, but to scale them up for long-term energy storage is cost prohibitive.[3] Electrochemical generation of hydrogen gas is an attractive medium for long-duration energy storage due to high energy and power densities, and excellent long-term stability.[1] Using hydrogen gas as an energy carrier also decouples energy storage from the energy-conversion device, which is especially advantageous for large-scale energy storage due to the lower costs.[1,2,4–7] Affording the flexibility to make hydrogen gas when surplus renewable electricity is available at lower price and be able to deploy it at a moment's notice is the advantage to these systems. Potentially, the most cost-effective route to utilize hydrogen gas as the renewable energy carrier is by using a low-temperature unitized regenerative fuel cell (URFC).[4–6,8–14] Specifically, exploring vapor-fed URFCs can provide insight into the feasibility of these hydrogen batteries to solve energy resiliency issues in off-grid and water-scarce applications.

In a reversible fuel cell (RFC), a fuel cell (FC) and water electrolyzer (WE) can be combined to form a hydrogen battery system.[15–17] A unitized regenerative fuel cell (URFC) combines the FC and WE functionality into a single device, which significantly reduces capital expenses (capex).[15] URFCs can operate in two configurations,[5] constant gas (CG) and constant electrode (CE). The CE configuration illustrated in Fig. S1 (available online at stacks.iop.org/JES/169/054514/mmedia) has been studied more in recent years,[5,8,18,19] and is capable of higher efficiency than CG, but at the expense of lower lifetimes since the electrodes are exposed to a larger range of potentials leading to the electrodes degrading rapidly over time.[18] The CG configuration, while sacrificing efficiency, is capable of longer lifetimes and much faster switching times. In this paper, we focus on the CG configuration, illustrated in Fig. 1, where both oxygen reactions (Eqs. 1 and 2): reduction (ORR) and evolution (OER), occur at one electrode, and both hydrogen reactions (Eqs. 3 and 4): oxidation (HOR) and evolution (HER), occur at the opposite electrode.

$$\text{ORR: } O_2 + 4H^+ + 4e^- \rightarrow 2H_2O \quad [1]$$

$$\text{OER: } 2H_2O \rightarrow O_2 + 4H^+ + 4e^- \quad [2]$$

$$\text{HOR: } 2H_2 \rightarrow 4H^+ + 4e^- \quad [3]$$

$$\text{HER: } 4H^+ + 4e^- \rightarrow 2H_2 \quad [4]$$

As a result of this configuration, the device itself does not have a fixed anode and cathode; rather, the O_2 electrode acts as the cathode during FC operation and the anode during WE operation, while the H_2 electrode acts as the anode during FC operation and the cathode during WE operation. Operating in this configuration minimizes the switchover time between FC and WE operation and minimizes combustion risk by completely isolating H_2 and O_2.

As shown in Fig. 1b, a PEM-URFC consists of a membrane-electrode assembly (MEA), including two electrodes separated by a proton-conducting membrane which acts as a solid polymer electrolyte. Proton exchangage membrane (PEM) devices typically employ perfluorinated sulfonic-acid membranes (PFSA) comprised of an inert polymer backbone and side chains terminated with sulfonic acid groups which absorb water, thereby creating channels through which protons can be shuttled between the two electrodes. At each

[=]Equal Contributions.
[a]Currently a graduate student in the Department of Chemical Engineering, Columbia University, New York, NY 10027, United States of America.
[z]E-mail: julie_fornaciari@berkeley.edu

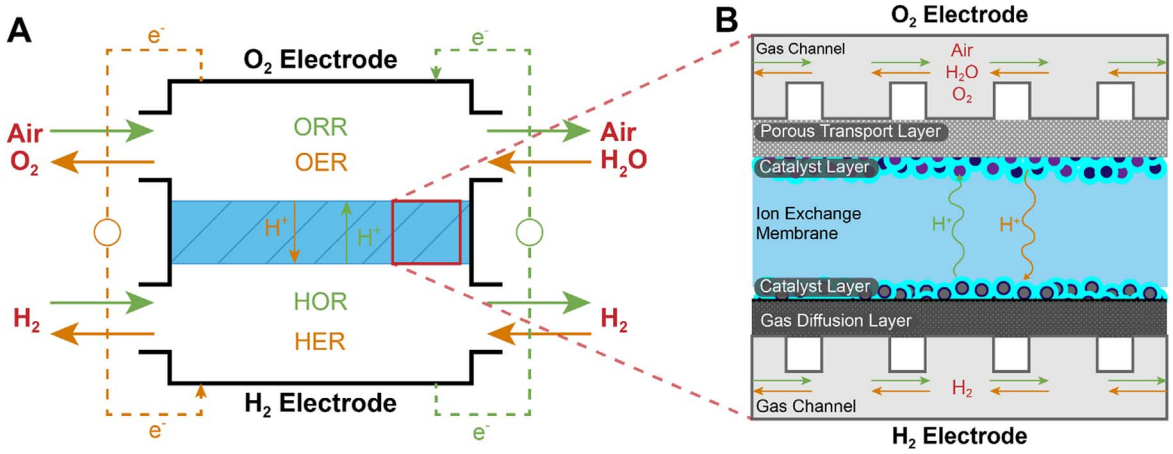

Figure 1. (a) Vapor-URFC schematic for constant-gas mode. (b) A cross section of the MEA used in the vapor-URFC. The water shown entering in the oxygen electrode is vapor phase and a hydrogen inlet is not needed for HER but could be fed in.

electrode there is a transport layer, either carbon gas-diffusion layer (GDL) or titanium porous-transport layer (PTL), to facilitate the transport of gaseous species to and from the catalyst layers where the electrochemical reactions take place. The catalyst layers for the hydrogen and oxygen electrodes are comprised of catalysts, ionomer, and open pores. The oxygen-electrode catalyst layer must have two catalysts, one for OER and one for ORR. In contrast, the hydrogen-electrode catalyst uses one catalyst, Pt/C, which catalyzes both HOR and HER. Thus far, research in the URFC field has been generally aimed at developing catalysts and tuning their structures,[20–22] integrated catalyst-layer structure,[16,19,23,24] porous-transport layers,[25–27] and membrane chemistry.[28] These factors also contribute to the overall cell efficiency and performance.[23,27]

The conventional URFC uses a liquid feed, which provides enough water for optimal proton conduction through the membrane and assures there is enough water for the reaction and hydration in WE operation. Using water vapor as a feed in place of liquid water eliminates the need for ultra-high purity deionized water, thereby simplifying operation and reducing operating and capital costs (opex and capex, respectively) at the expense of higher ohmic and transport losses through the membrane and cell. Removing the need of ultra-pure water also eliminates the need for ion exchange resins for water purification and pumps.[29,30] Additionally, bubble formation in liquid-water fed WE complicates transport within the system by introducing multiphase flow. Vapor-fed operation eliminates these complexities and also removes the need for liquid water to be purged from the system when switching from WE to FC operation. While vapor-fed WE generates higher mass-transport overpotentials than liquid-fed,[31] the FC operation would be at an advantage as water management would be better controlled and pore-flooding at the start of operation would be avoided.[32–37] Water management is important for these technologies and will be complicated by differential pressurization and need to be optimized, especially as electrolysis and fuel cell mode have divergent criteria.

Table I. The catalyst recipe for the hydrogen electrode and oxygen electrode.

Component	H_2 Electrode Ink	O_2 Electrode Ink
Pt/C (46.2 wt% Pt)	65.22 mg	n/a
Pt Black	n/a	25.00 mg
Ir Black	n/a	25.00 mg
H_2O	17.60 g	10.00 g
n-PrOH	16.08 g	14.09 g
EtOH	n/a	7.89 g
Nafion™ D521	422.61 mg	116 mg

While vapor operation can simplify to a certain extent, there are other materials solutions such as including amphiphilic diffusion layers and actively removing water from the feed. Additionally, humid ambient air can be used as a feed in both operating modes, supplying oxygen during FC operation and water vapor during WE operation. This operation eliminates the need for water purification and minimizes the switch-over time between operating modes, which brings the vapor-URFC on par with a typical battery for the balance of plant. The only storage needed is for the hydrogen gas.

This simplified operation makes the vapor URFC an attractive device in scenarios where small-scale, high-density, long-term energy storage is necessary. The advantages in such scenarios may outweigh the performance penalty incurred by using water vapor as a feed due to greater ohmic losses within the MEA. Namely, this device shows exceptional promise for off-grid energy storage in humid environments, as well as for energy storage on spacecraft and extraterrestrial habitats.

Currently, there is a gap in the literature for investigating vapor-fed URFCs, their operating capabilities, and their applications. In this study, we baseline the performance of a vapor-fed URFC and explore how different membrane ion-exchange capacities and feed relative humidities enhance or inhibit the cell performance, specifically the roundtrip efficiency. Additionally, we apply durability protocols to assess the lifetime of such a cell. Additionally, exploring two such applications, off-grid and extraterrestrial, we demonstrate this device's feasibility for operation and identify additional optimization parameters.

Methods

Catalyst-coated-membrane fabrication.—Catalyst inks are comprised of catalyst particles, solvent, and ionomer. The catalyst inks for each electrode are detailed in Table I. The H_2 electrode inks contain Pt/C (46.2 wt% Pt on HSC, Tanaka, Japan), with a 1:1 n-propanol (200 proof, Koptec, Pennsylvania, USA) to deionized (DI) water (18.2 MΩ, Milli-Q, EMD Millipore, Massachusetts, USA) mixture, by volume. The ionomer used was a 5 wt% Nafion™ dispersion (D521, Chemours, Delaware, USA) with an ionomer to carbon ratio of 0.6. The O_2 electrode inks contain a mixture of iridium black (SA = 100, Tanaka, Japan) and platinum black (Tanaka, Japan) and used a 2:1:1 n-propanol:water:ethanol solvent mixture. The same ionomer was used in the O_2 electrode ink as the H_2 electrode ink, but the ionomer to catalyst ratio was 0.116.[24] For the H_2 electrode ink, the vial was manually shaken before sonicating in a bath sonicator (M1800, Branson, Connecticut, USA) equipped with a chiller (Grant) for 30 min at 10 °C. For the O_2 electrode ink, the vial was manually shaken and sonicated using a probe-tip

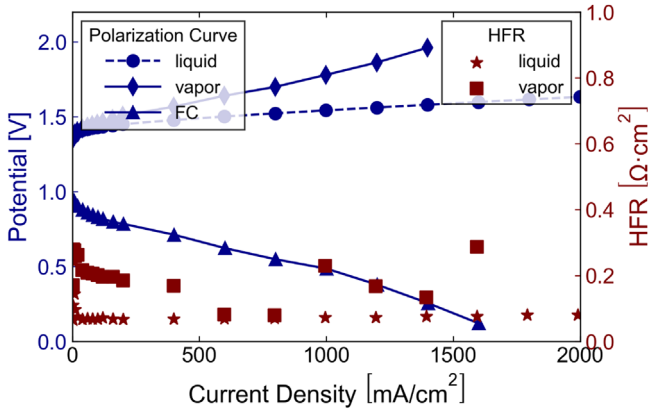

Figure 2. Vapor WE performance is compromised relative to the liquid WE due to greater ohmic losses. The left axis corresponds to WE performance, and the right axis shows the WE HFR.

sonicator (CPX500, Cole-Parmer, Illinois, USA) with the vial submerged in an ice bath and covered with parafilm to prevent solvent evaporation during sonication.

The Nafion™ (NR-212, Chemours, Delaware USA) and Aquivion® (E87–05S; E98–05S, Solvay, Belgium) PFSA membranes were conditioned by boiling in DI water at 100 °C for one hour before being allowed to cool to room temperature and stored in DI water.

To prepare a 5 cm^2 catalyst-coated membrane (CCM), the membrane is placed on a protective fiberglass sheet and heated on the hotplate of the ultrasonic spray-coater (Sono-Tek Exacta Coater, New York, USA) under a Teflon-coated fiberglass mask and a rubber gasket. The membrane was dried at 80 °C under vacuum prior to spraying the catalyst ink. For the H_2 electrode, 10 ml of ink was sprayed at a deposition rate of 0.3 ml min^{-1} to achieve a catalyst loading of 0.3 mg cm^{-2}. For the O_2 electrode, 30 ml of ink was sprayed at a deposition rate of 0.35 ml min^{-1} to achieve a total catalyst loading of 1 mg cm^{-2}.

Cell assembly.—Carbon-paper gas-diffusion layers (GDLs) with a microporous layer (MPL) (Sigracet 29BC, Fuel Cell Store, Texas, USA) were used for the H_2 electrode, and titanium porous-transport layers (Ti-PTL) (NEL Hydrogen, Connecticut) were used for the O_2 electrode. The Ti-PTLs were soaked in a dilute Teflon solution and dried on a vacuum hot plate at 100 °C to deposit the desired amount of PTFE, 5 wt%, onto the PTL. The PTLs were then baked in a tube furnace at 400 °C in Argon to crystalize the PTFE. PTFE gaskets (McMaster-Carr, Illinois, USA) were used on both sides, the PTFE gasket is thickness matched to the Ti-PTL, and 20% compression of the carbon GDL. Electrochemical cells from Fuel Cell Technologies (FCT, New Mexico, USA) equipped with graphite serpentine flow fields and gold-plated copper current collectors were used for testing. Graphite serpentine flow fields were used to assure no leaks are occurring in the system and when tested and compared to titanium flow fields, there was no change in performance. Graphite flow fields showed minimal oxidation under the testing conditions and duration on both the H_2 and O_2 sides.[31]

Cell testing.—A potentiostat (Biologic, France) with electrochemical-impedance-spectroscopy capabilities and a 20 A booster was used for all electrochemical tests, and a fuel-cell test stand (FCT) was used to regulate cell operating conditions and feed gases. The cell was heated with FCT rod heaters, and a thermocouple in the endplate of the cell was used to maintain the cell at 80 °C throughout testing. The gas feed lines were maintained at 85 °C throughout testing, and DI water was used to humidify the gases before being fed to the cell. To note, these tests are run to assure better membrane hydrogen on the cathode and the humidity remains at 100% RH. However, in actual operation, running the system with high humidity on the hydrogen side would require an extra step of drying the system and could lead to lower overall system efficiency.

Prior to FC testing, the cell was conditioned by running chronoamperometry (CA) at 100 mV cell potential for 16 to 20 hr until the current stabilizes with air flowing at 700 ml min^{-1} at the O_2 electrode and H_2 flowing at 300 ml min^{-1} at the H_2 electrode, and no applied backpressure. The flow rates were then increased to 1000 and 450 ml min^{-1} at the oxygen and hydrogen electrodes, respectively, and the backpressure at both electrodes was set to 21 psi. High stoichiometric feeds were used to test the system to maintain differential conditions. For example, the stoichiometric feed was 5 for hydrogen and 10 for air at 1 A cm^{-2}. However, it is important to note that these are not practical operating conditions. To assess FC performance, a series of constant current holds were carried out: 1 min current holds were used for current densities below 0.2 A cm^{-2}, and 3 min current holds were used for current densities at or above 0.2 A cm^{-2}. The current was ramped up in steps of 20 mA cm^{-2} or 200 mA cm^{-2}, within the kinetic or ohmic regimes, respectively. The cell potential was averaged across the last 30 s of each step and across the ramp-up and ramp-down holds to generate a polarization curve. Electrochemical impedance was measured at every current density to generate a Nyquist plot, where the intercept with the real axis is the measured high frequency resistance (HFR) of the cell.

For WE testing, the flow rates were set to 450 ml min^{-1} of N_2 (corresponding to a stoichiometric feed of 10 at 1 A cm^{-2}) at the O_2 electrode and 100 ml min^{-1} of H_2 at the H_2 electrode. Flowing H_2 during electrolysis operation helps establish a stable reference electrode. Performance was assessed in a similar manner as FC mode, with the current increased stepwise from 5 mA cm^{-2} until the cell potential reaches 2.1 V before ramping back down, as shown in Fig. S2. Polarization curves were generated using the same method as FC polarization curves. The data analysis was performed using a Python code to generate the polarization curve, high-frequency resistance (HFR), and Tafel slope.[38]

Accelerated stress tests (ASTs) were performed on the down-selected MEA to assess the durability and stability of the vapor URFCs.[39,40] A sawtooth cycling profile was used, with the potential limits set to 0.55 V and 1.55 V and a scan rate of 300 mV sec^{-1}.[15] These limits were chosen as they correspond to current densities of approximately −1 and 1 A cm^{-2}, respectively. At regular and convenient intervals, the cycling was stopped, and FC and WE performance were assessed using the methods described above. The cycling continued until the cell no longer achieved a current density of 1 A cm^{-2} in either FC or WE mode, which was designated as the end of life (EOL).

Results and Discussion

Liquid-water vs water-vapor performance.—To compare URFC performance with a liquid-water feed to that of a water-vapor feed for WE operation, CCMs were prepared with a Nafion™ 1100 membrane. Since the FC operation is usually operated with highly humidified gases, we initially compare the WE performance. As illustrated in Fig. 2, the performance using a water-vapor feed is significantly reduced compared to that using liquid water. The vapor-fed URFC requires 1.78 V at 1.0 A cm^{-2} whereas the liquid-fed URFC reached the same current density at 1.54 V. One major difference between the two feeds is the HFR. The HFR increases with increasing current density for the vapor-fed cell, indicating larger ohmic losses at elevated current densities. The HFR for the liquid-fed cell remains low and constant (0.09 Ω cm^2). Vapor electrolysis shows higher ohmic losses due to membrane dehydration and localized mass-transport limitations in the catalyst layer.[31] Regardless, the vapor-fed URFC achieved 42% roundtrip efficiency (RTE, calculations are in the SI) at 1 A cm^{-2}. The liquid-fed cell can

achieve >50% for the RTE at 1 A cm^{-2}, although engenders a more complicated balance of plant and switching time between operation modes. A table comparing the different RTEs achieved in literature is in the SI.

Membrane comparison (1100 vs 980 vs 870).—While maintaining a constant membrane thickness (50 μm), we explore the effects of equivalent weight (EW) on URFC performance and efficiency using 3 membranes (Fig. 3). A membrane's EW is equal to the moles of water per ionic group, which is inversely proportional to the ion-exchange capacity.[28] Lower EW membranes were expected to improve device performance because the higher fraction of ionic groups should lead to high water uptake and thereby improve membrane hydration.[28] Better membrane hydration reduces ohmic losses across the membrane, resulting in lower overpotential; however, as shown in Fig. 3, Nafion™ 1100 exhibited the best performance of the three membranes tested, achieving 42% ± 2% RTE at 1 A cm^{-2}. Every RTE is shown in Fig. 3b, in order to compare at various current densities for different operations. The trend continues in the direction of lower EW leading to higher overpotentials. The HFR for Aquivion® 870 was significantly higher than that for both Nafion™ 1100 and Aquivion® 980, suggesting that higher ohmic losses can account for the majority of the poor performance of this membrane. However, the HFRs for Aquivion® 980 and Nafion™ 1100 were similar for FC operation, differing some in WE operation. While the HFR differs in WE operation, other factors may result in the poorer performance of Aquivion® 980. Those factors may include different mass transport within the MEA or membrane swelling impacting the amount of electrochemically active catalyst in the layer, as the lower the EW results in higher swelling.[41,42] Additionally, using the Nafion ionomer in the catalyst layer with Aquivion membranes could lead to a mass transport loss due to the ionomer/membrane interface.

Relative-humidity experiments.—Regardless of whether the performance loss associated with the Aquivion® membranes can be attributed to membrane swelling or an interfacial loss, reducing the amount of water available as the reactant should result in performance loss for a system. Ideally, real-life applications would result in the cells operating at less than 100% relative humidity (RH). Quantifying the loss due to the reduction in water availability can provide a guide for lower-humidity applications. Therefore, all three membranes were tested at RHs ranging from 52% to 122% RH at 80 °C to gain insight into the importance of the rate of water fed into the vapor-fed URFC and the comparison to the liquid electrolyzer, highlighted in Fig. 4. As discussed earlier, decreasing membrane hydration increases ohmic overpotentials and in a vapor-fed system is dependent on the vapor pressure. As shown in Fig. 4, the difference in potential was minimal at higher RHs, including the oversaturated case at 122%. The oversaturated test did not result in performance enhancement approaching the liquid electrolysis. Instead, oversaturated feed resembles the 100% RH vapor electrolysis, which indicates that although there is more water available to react, the system is still limited by other factors. The higher RH could lead to some condensing in the channels of the cell and the local RH at the MEA may be lower, something to explore in future work and is out of the scope of this paper.

As expected, the largest loss in performance is observed for the 52% RH test, showing a non-monotonic increase in potential with current density. Decreasing the RH reduces the amount of water available for the oxygen-evolution reaction and membrane hydration. This decrease in water content manifests in the decrease in RTE from 42% at 100% RH to 37% RTE at 52% RH. Across the full range of RHs, Nafion™ 1100 exhibited the best performance relative to either Aquivion® membrane, regardless of the RH. Nafion™ 1100 exhibited an RTE of 37% at 52% RH, while Aquivion® 870 had an RTE of 33% at 122% RH. The difference between these tests is revealed when comparing the EW and the respective HFR at 100% RH, as shown in Fig. 3, revealing that for higher EW membranes, less water is available to react in the vapor phase even at high RHs.

Durability.—ASTs were used to assess device durability and to mimic the start-up/shut-down of these systems at both 100% RH and 75% RH to observe two different durability cases, shown in Fig. 5. Although beginning-of-life (BOL) performance is similar for the 100% and 75% cases (42% and 38% RTE, respectively), degradation occurs more rapidly at 75% RH as the lower humidity is a stressor in FC and WE operation. As shown in Fig. 5a at 100% RH, the cell retained 78% of BOL performance after 7,000 charge/discharge cycles and 52% of BOL performance after 20,000 cycles, with EOL after 50,000 cycles. EOL is defined here as the point at which the cell could no longer sustain a current density of 1 A cm^{-2}. In Fig. 5b, at 75% RH, the cell retained 76% of BOL performance after 1,000 charge/discharge cycles and 37% of BOL performance after 7,000 cycles, with EOL after 20,000 cycles. Converting these cycle lifetimes into temporal lifetimes depends on the duty cycle in operation. For example, assuming a daily duty cycle resulting from load-shifting solar power in off-grid applications, the 100% RH and 75% RH cells would retain approximately 75% of BOL performance after 19 years and 3 years, respectively.

In both cases, WE performance remained constant for the duration of the AST, indicating that a loss of FC performance drives efficiency loss.[15] Figure S3 illustrates the detailed evolution of device performance over the course of the AST at 100% RH. As shown in Fig. S4, the voltage-loss breakdown for the FC performance indicates the kinetic and mass-transport loss is a large fraction of the voltage loss seen at EOL (Fig. S5 shows the WE operation applied-voltage breakdown). We acknowledge that the AST protocol may not account for all degradation mechanisms that would occur

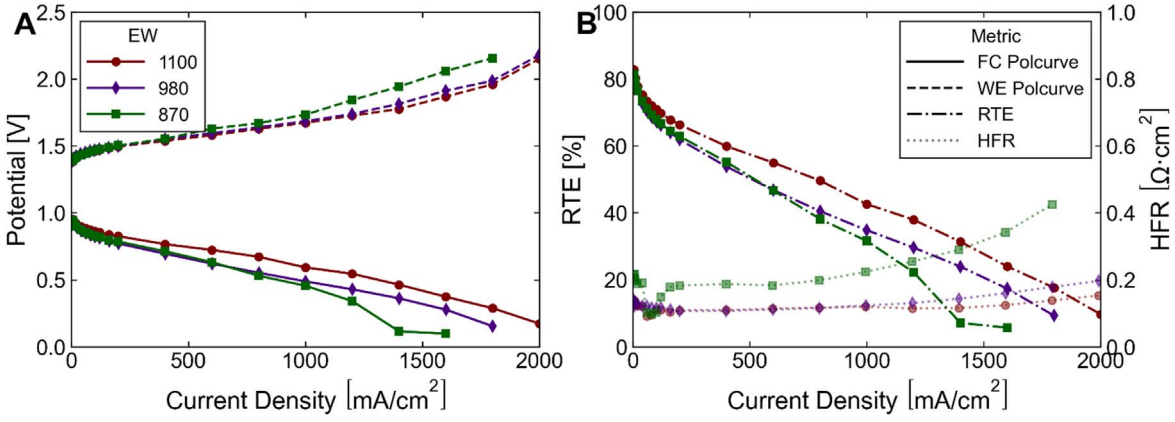

Figure 3. (a) Polarization curves during both FC (solid) and WE (dashed) operation for MEAs using the three membranes tested. (b) RTE (dash-dot) and HFR during FC operation (dotted) for MEAs using the three membranes tested.

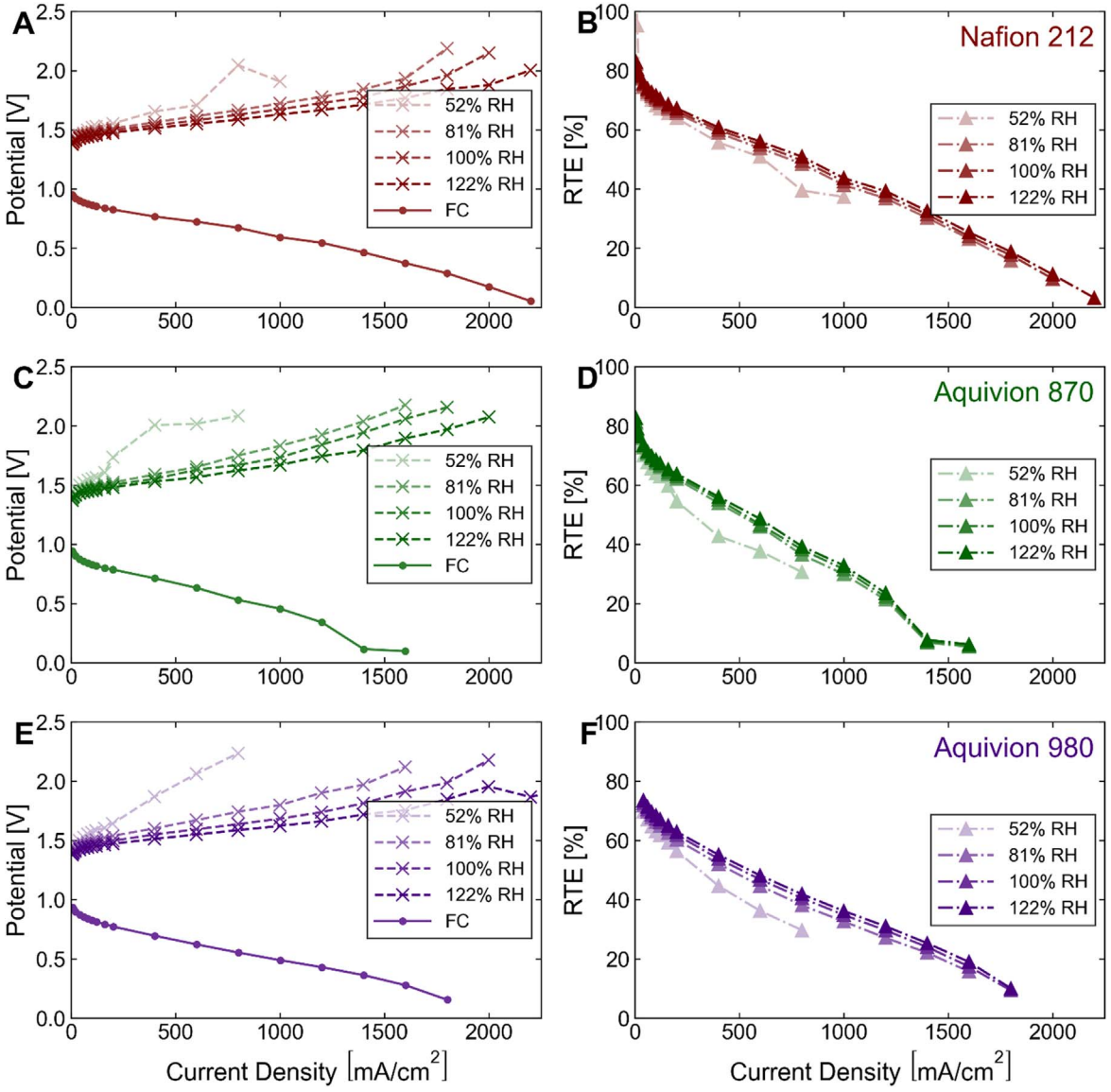

Figure 4. (a) Nafion™ 1100 WE performance between 81 to 122% RH, with a significant drop off at 52% RH. (b) RTE for Nafion™ 1100 at the different RH feeds. (c) Aquivion™ 870 WE performance between 52 to 122% RH. (d) RTE for Aquivion™ 870 at the different RH feeds. (e) Aquivion™ 980 WE performance between 52 to 122% RH. (f) RTE for Aquivion™ 980 at the different RH feeds.

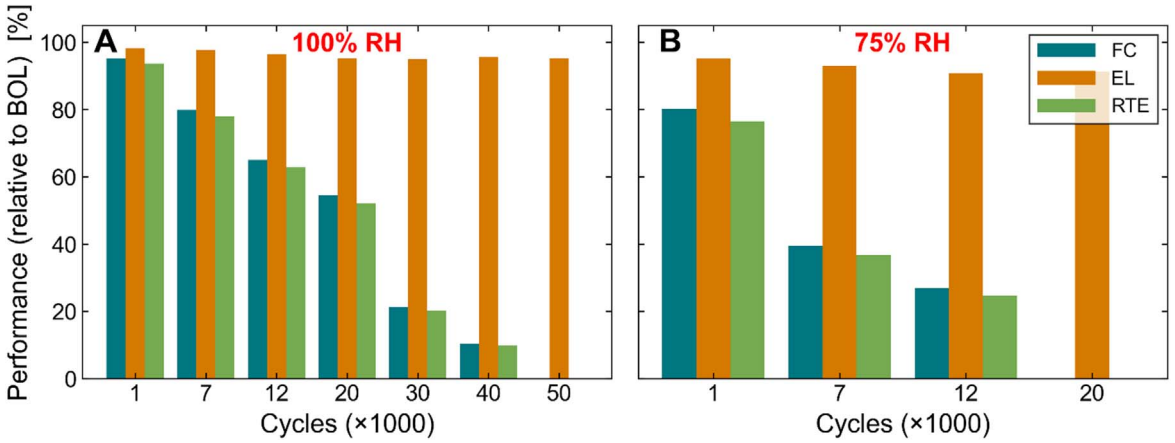

Figure 5. AST cycles and performance compared to the beginning of life (BOL) for the vapor-URFC at (a) 100% RH and (b) 75% RH.

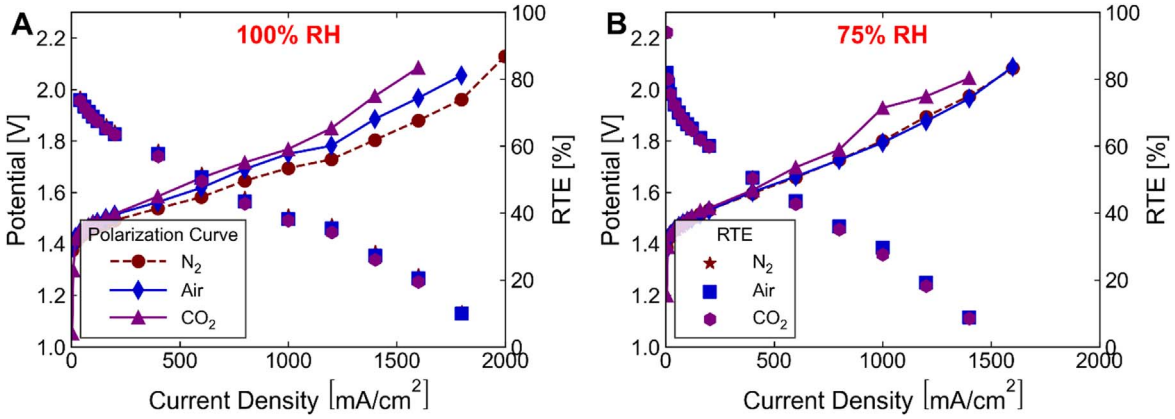

Figure 6. The electrolyzer polarization curve and RTEs for vapor-URFCs using nitrogen, air, and carbon dioxide at the oxygen electrode at (a) 100% RH and (b) 75% RH.

during a realistic 24 h charge/discharge cycle; however, these results are promising and suggest that this type of device could be used for the applications discussed in this paper.

Impact of oxygen carrier gas.—The vapor-URFC is most desirable for off-grid or extraterrestrial applications as the balance of plant is minimized and can provide on-demand hydrogen and electricity. For off-grid applications, operating at ambient humidity is necessary since the air would not be humidified further before feeding it to the URFC. However, as shown in Fig. 4, the limitation on the electrolyzer performance is already drastic at 52% RH. These losses seen at 52% RH could be mitigated by controlling water management within the cell and better utilization of the catalyst layer.[31] Further optimization of the MEA and technoeconomic analysis is required for fully understanding how this technology can be used as an off-grid long-term energy storage system.

When evaluating different applications, such as extraterrestrial, the feed gas at the oxygen electrode is another consideration. Humidifying air or carbon dioxide as a carrier gas could be other opportunities to utilize different ambient feeds. As shown in Fig. 6, at both 100% and 75% RH, there was no significant change in RTE when air was used during WE operation in place of N_2, indicating that it is not necessary to switch from air to an inert gas at the O_2 electrode when switching from FC to WE operation. As shown in Fig. 6a, the electrolyzer polarization curves increases by 55 mV at 1 A cm^{-2} when using air versus nitrogen, which can be accounted for by the slight change in diffusivity.[31] By maintaining constant gas flows at both electrodes, the device will be much simpler and more reliable for off-grid energy storage.

For applications in spacecraft and extraterrestrial habitats, it would be desirable to use humid CO_2 as a carrier gas during WE. Air would be a precious resource and repurposing captured CO_2 from human respiration would eliminate the need for carrying a source of nitrogen and all of the requisite supporting equipment (tanks, etc.). Additionally, operating at lower RH is better since water is also a limited resource. Figure 6a shows at both 100% RH (Fig. 6b shows the performance for 75% RH), there was no significant change in RTE when CO_2 was used during WE operation in place of N_2, indicating that CO_2 is a viable carrier gas for water vapor during WE operation. A disadvantage to using CO_2 as the feed gas is when this URFC is run at high pressures, hydrogen could potentially interact with CO_2 and lead to catalyst poisoning. Further testing with CO_2 as the pressurized feed gas is required to assure catalyst poisoning does not happen. Additionally, it may be desirable to use either air or pure O_2 during FC operation depending on the availability of gases and/or to improve device performance.

Summary

In this study, we presented a parametric study of vapor-URFC components and operating conditions, focusing on membrane EW, the feed RH, and the oxygen-electrode carrier gas. We found that a higher equivalent weight membrane correlates with improved device performance, most likely as a result of better water transport and less swelling of the membranes during operation. When operating at 100% RH, the vapor-URFC achieved an RTE of 42% ± 2%, which is comparable to the state-of-the-art for vapor-URFC to date. The device still achieved 37% RTE at 52% RH, indicating that the device is robust over a wide range of RHs. The vapor-URFC exhibited excellent long-term stability and sustained 1 A cm^{-2} for 50,000 and 20,000 AST cycles at 100% and 75% RH, respectively. The device performance was also agnostic to the oxygen electrode carrier gas, which emphasizes the flexibility of this device to fit niche markets. Specifically, proof-of-concept results using air and CO_2 as carrier gases demonstrate the viability of the vapor-URFC for off-grid and extraterrestrial applications.

Acknowledgments

The authors acknowledge the Department of Energy—Office of Energy Efficiency and Renewable Energy—Fuel Cell Technologies Office (DOE-EERE-FCTO) and program managers Greg Kleen and Dimitrios Papageorgopoulos for funding under Contract Number DE-AC02–05CH11231. JCF and SG thank the National Science Foundation (grant DGE 1106400 and grant 2021322071, respectively) for support. The authors thank Proton OnSite/NEL Hydrogen for Ti PTLs. JCF, YNR, XP, and ND designed and created the idea of the work. JCF and SG conducted experiments. JCF, SG, and ND composed the manuscript, and all authors edited the written work.

ORCID

Julie C. Fornaciari https://orcid.org/0000-0002-0473-2298
Samay Garg https://orcid.org/0000-0002-9872-6429
Xiong Peng https://orcid.org/0000-0001-8737-5830
Yagya N. Regmi https://orcid.org/0000-0001-6588-7683
Adam Z. Weber https://orcid.org/0000-0002-7749-1624
Nemanja Danilovic https://orcid.org/0000-0003-2036-6977

References

1. O. Krishan and S. Suhag, *Int. J. Energy Res.*, **43**, 6171 (2019).
2. T. M. Gür, *Energy Environ. Sci.*, **11**, 2696 (2018).
3. A. R. Dehghani-Sanij, E. Tharumalingam, M. B. Dusseault, and R. Fraser, *Renew. Sustain. Energy Rev.*, **104**, 192 (2019).
4. M. Gabbasa, K. Sopian, A. Fudholi, and N. Asim, *Int. J. Hydrogen Energy*, **39**, 17765 (2014).
5. B. Paul and J. Andrews, *Renew. Sustain. Energy Rev.*, **79**, 585 (2017).
6. Y. Wang, D. Y. C. Leung, J. Xuan, and H. Wang, *Renew. Sustain. Energy Rev.*, **65**, 961 (2016).
7. Y. Wang, D. Y. C. Leung, J. Xuan, and H. Wang, *Renew. Sustain. Energy Rev.*, **75**, 775 (2017).
8. S. A. Grigoriev, P. Millet, V. I. Porembsky, and V. N. Fateev, *Int. J. Hydrogen Energy*, **36**, 4164 (2011).

9. T. Sadhasivam, K. Dhanabalan, S. H. Roh, T. H. Kim, K. W. Park, S. Jung, M. D. Kurkuri, and H. Y. Jung, *Int. J. Hydrogen Energy*, **42**, 4415 (2017).
10. P. Millet, R. Ngameni, S. A. Grigoriev, and V. N. Fateev, *Int. J. Hydrogen Energy*, **36**, 4156 (2011).
11. H. Ito, N. Miyazaki, M. Ishida, and A. Nakano, *Int. J. Hydrogen Energy*, **41**, 5803 (2016).
12. T. Yoshida and K. Kojima, *Interface magazine*, **24**, 45 (2015).
13. M. Hunsom, D. Kaewsai, and A. M. Kannan, *Int. J. Hydrogen Energy*, **43**, 21478 (2018).
14. S. Choi, T. C. Davenport, and S. M. Haile, *Energy Environ. Sci.*, **12**, 206 (2019).
15. Y. N. Regmi, X. Peng, J. C. Fornaciari, M. Wei, D. J. Myers, A. Z. Weber, and N. Danilovic, *Energy Environ. Sci.*, **13**, 2096 (2020).
16. X. Peng et al., *Energy Environ. Sci.*, **13**, 4872 (2020).
17. C. Duan, R. Kee, H. Zhu, N. Sullivan, L. Zhu, L. Bian, D. Jennings, and R. O'Hayre, *Nat. Energy*, **4**, 230 (2019).
18. J. Ahn and R. Holze, *J. Appl. Electrochem.*, **22**, 1167 (1992).
19. S. A. Grigoriev, P. Millet, K. A. Dzhus, H. Middleton, T. O. Saetre, and V. N. Fateev, *Int. J. Hydrogen Energy*, **35**, 5070 (2010).
20. T. Sadhasivam, G. Palanisamy, S. H. Roh, M. D. Kurkuri, S. C. Kim, and H. Y. Jung, *Int. J. Hydrogen Energy*, **43**, 18169 (2018).
21. G. Chen, S. R. Bare, and T. E. Mallouk, *J. Electrochem. Soc.*, **149**, A1092 (2002).
22. Y.-J. Wang, B. Fang, X. Wang, A. Ignaszak, Y. Liu, A. Li, L. Zhang, and J. Zhang, *Prog. Mater Sci.*, **98**, 108 (2018).
23. G. C. da Silva, K. J. J. Mayrhofer, E. A. Ticianelli, and S. Cherevko, *J. Electrochem. Soc.*, **165**, F1376 (2018).
24. M. Bernt and H. A. Gasteiger, *J. Electrochem. Soc.*, **163**, F3179 (2016).
25. R. Omrani and B. Shabani, *Int. J. Hydrogen Energy*, **44**, 3834 (2019).
26. H. Ito, K. Abe, M. Ishida, C. M. Hwang, and A. Nakano, *Int. J. Hydrogen Energy*, **40**, 16556 (2015).
27. G. Bender et al., *Int. J. Hydrogen Energy*, **44**, 9174 (2019).
28. A. Kusoglu and A. Z. Weber, *Chem. Rev.*, **117**, 987 (2017).
29. C. Xiang, K. M. Papadantonakis, and N. S. Lewis, *Mater. Horiz.*, **3**, 169 (2016).
30. A. Ursua, L. M. Gandia, and P. Sanchis, *Proc. IEEE*, **100**, 410 (2012).
31. J. C. Fornaciari, M. R. Gerhardt, J. Zhou, Y. N. Regmi, N. Danilovic, A. T. Bell, and A. Z. Weber, *J. Electrochem. Soc.*, **167**, 104508 (2020).
32. M. Grimm, M. Hellmann, H. Kemmer, and S. Kabelac, *Fuel Cells*, **20**, 477 (2020).
33. S. G. Kandlikar, *Heat Transfer Eng.*, **29**, 575 (2008).
34. P. Berg, K. Promislow, J. St. Pierre, J. Stumper, and B. Wetton, *J. Electrochem. Soc.*, **151**, A341 (2004).
35. T. V. Nguyen and M. W. Knobbe, *J. Power Sources*, **10**, 70 (2003).
36. C. Zhang, W. Zhou, L. Zhang, S. H. Chan, and Y. Wang, *Int. J. Hydrogen Energy*, **40**, 4666 (2015).
37. M. Kim, N. Jung, K. Eom, S. J. Yoo, J. Y. Kim, J. H. Jang, H. Kim, B. K. Hong, and E. Cho, *J. Power Sources*, **266**, 332 (2014).
38. S. Garg, J. Fornaciari, A. Weber, and N. Danilovic, *JOSS*, **6**, 2940 (2021).
39. C. Lim, L. Ghassemzadeh, F. V. Hove, M. Lauritzen, J. Kolodziej, G. G. Wang, S. Holdcroft, and E. Kjeang, *J. Power Sources*, **257**, 102 (2014).
40. M. P. Rodgers, L. J. Bonville, H. R. Kunz, D. K. Slattery, and J. M. Fenton, *Chem. Rev.*, **112**, 6075 (2012).
41. A. Kusoglu, B. L. Kienitz, and A. Z. Weber, *J. Electrochem. Soc.*, **158**, B1504 (2011).
42. C. Arthurs and A. Kusoglu, *ACS Appl. Energy Mater.*, **4**, 3249 (2021).